WELDING RESEARCH

SUPPLEMENT TO THE *WELDING JOURNAL*, NOVEMBER 2002
Sponsored by the American Welding Society and the Welding Research Council

The Effect of Multiple Postweld Heat Treatment Cycles on the Weldability of Waspaloy®

Changes in grain boundary character distribution after multiple PWHT cycles were found to affect HAZ liquation cracking during repair welding

BY M. QIAN AND J. C. LIPPOLD

ABSTRACT. The heat-affected-zone (HAZ) liquation cracking susceptibility of wrought Waspaloy® subjected to simulated, multiple postweld heat treatment (PWHT) cycles was evaluated using hot ductility testing. The behavior of both a wrought bar material and a forged turbine disk was evaluated. A long-term isothermal heat treatment was used to simulate multiple PWHT cycles that Waspaloy turbine engine components would experience during periodic weld repair. The weldability degradation of Waspaloy after a 1079°C/40-h heat treatment is primarily due to increased grain size from long-term, elevated-temperature exposure. The finer grain size of the wrought bar accounted for its minimal degradation of weldability, while coarse grains resulted in a drastic deterioration of weldability in the forged disk. The degradation of weldability is associated with the short-time, high-temperature grain boundary (GB) weakening resulting from MC-type carbide constitutional liquation and segregation-induced GB liquation in the simulated HAZ of Waspaloy materials. A 1079°C/100-h treatment resulted in a restoration of the weldability of the forged disk even with comparable coarse grain size to that of simulated 1079°C/40-h treated material. The effect of grain size and the fraction of special grain boundaries on the HAZ liquation cracking behavior is discussed with regard to the simulated multiple PWHT cycles.

Introduction

Weld repair of aircraft gas turbine engine components, including blades, buckets, and static (nonrotating) components has become increasingly prevalent as a means of extending engine life and reducing the costs associated with component replacement. As part of the repair welding process, the precipitation-hardened superalloys must undergo postweld heat treatment (PWHT) to restore their mechanical properties. Because components are subject to multiple repairs over their lifetimes, they are also exposed to multiple cycles of PWHT consisting of solution treatment followed by aging. It has been observed the weldability of some superalloys degrades after an accumulation of repair/PWHT cycles (Refs. 1–5). The purpose of this study was to develop a better understanding of the relationship between multiple PWHT cycles and the weldability of Waspaloy.

It should be noted material for this investigation was taken from a turbine rotor disk. Repair of disk materials by welding is generally not allowed and this paper does not suggest repair of these components be conducted. Rather, the disk was a ready source of Waspaloy material that exhibited metallurgical characteristics of interest in this investigation.

KEY WORDS

Waspaloy®
Postweld Heat Treatment (PWHT)
Weldability
Heat-Affected Zone (HAZ)
Liquation Cracking
Special Grain Boundary
Grain Size
Intergranular Fracture

Experimental Procedure

Two Waspaloy materials were used in this study. One was a wrought bar in the solution-annealed condition. The other was a forged aircraft turbine disk, 840 mm (31.5 in.) in diameter, with a bimodal grain structure (Ref. 6), provided in the fully heat-treated condition, i.e., solution heat treated at 1079°C (1975°F) and aged at 760°C (1400°F). The chemical compositions of these two materials are listed in Table 1.

Initially, the use of a long-term isothermal heat treatment to simulate multiple PWHT cycles was investigated to shorten the experimental period in sample preparation. The premise in the use of this approach was that the solution treatment employed in PWHT results in the metallurgical "degradation" of the material since the aging portion of the heat treatment is reversible, i.e., the aging precipitate, γ'–$Ni_3(Al,Ti)$, dissolves during the solutionizing portion of the PWHT cycle. Both Waspaloy bar and disk materials were used for the simulation with the following heat treatment conditions (Ref. 7): 1) 1079°C (1975°F)/4h for ten cycles with furnace cooling between cycles, and 2) an isothermal hold at 1079°C for 40 h. Both heat treatments were conducted in an argon-protected tube furnace. In addition, the 1079°C/40-h treatment was also conducted in air in a box furnace (BF) with air cooling for comparison. For the final long-term, isothermal heat treatments, the box furnace with no protective atmosphere was used to treat bulk Waspaloy materials. Test specimens were then machined from these bulk samples, so they were not affected by the surface oxidation of the bulk sample.

The weldability of Waspaloy materials

M. QIAN AND J. C. LIPPOLD are with The Ohio State University, Columbus, Ohio.

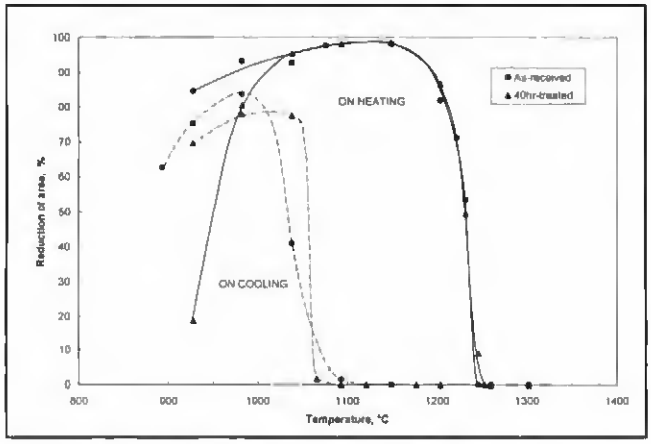

Fig. 1 — Gleeble™ hot-ductility "signatures" of Waspaloy bar.

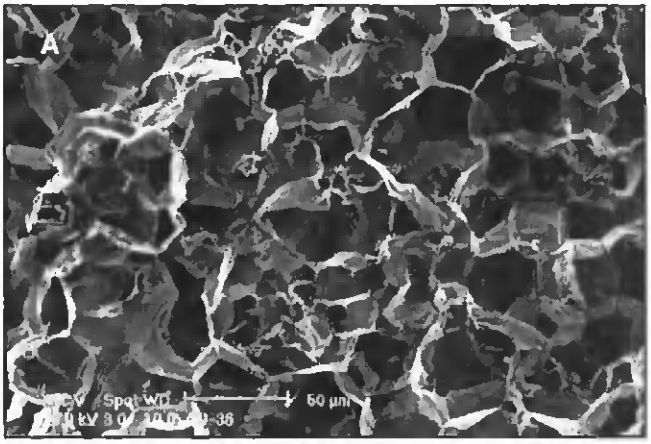

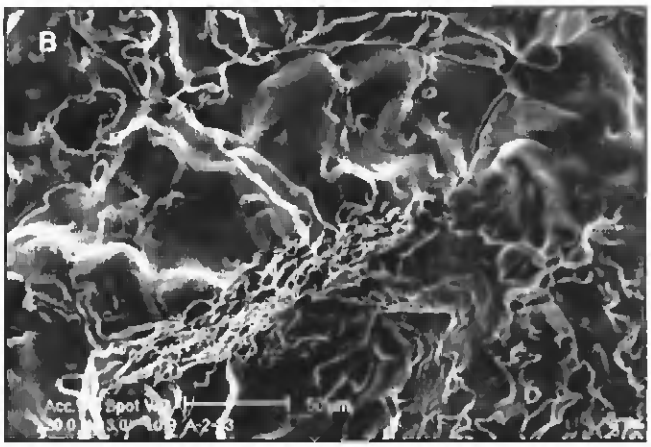

Fig. 2 — Fractography of the Waspaloy bar tested at the NDT showing IG features. A — As-received; B — 1079°C/40h-treated.

in both the as-received and simulated multiple PWHT conditions was evaluated using the Gleeble™ hot-ductility test. Test specimens were 6.35±0.05 mm (0.25±0.002 in.) in diameter and 100 mm (4 in.) in length, with threads on both ends. Samples were removed longitudinally in the bar and radially from the forged disk. A Type K (chromel-alumel) thermocouple was spot welded to the midpoint of the sample for temperature measurement and control. Heating and cooling rates followed thermal simulation parameters from a series of nickel-based superalloys used by previous researchers (Refs. 3–5, 8). The hot ductility testing conditions used a heating rate of 111°C/s (200°F/s), hold time at test temperature 0.5 s, cooling rate of 43°C/s (77°F/s), and stroke rate of 25 mm/s (1 in./s) to fracture the samples. All samples were tested in argon. Temperature, stroke, and load were continuously monitored throughout the test. Ductility, in terms of reduction of area of the fracture surface, was subsequently measured using a binocular microscope.

Hot ductility samples were examined using both optical microscopy and scanning electron microscopy (SEM). Electrolytic etching with 10% aqueous chromic acid was used to reveal microstructures of interest. For the hard-to-etch, long-term solution-treated materials, an etchant consisting of 15 mL HCl, 10 mL acetic acid, 10 mL HNO_3, and 2–5 drops of glycerol was used. Grain size was measured in Feret diameter (d_f) on digitally recorded optical images using ImageTool 2.0 (Ref. 9). Sufficient grains in three to five areas of each sample were counted to yield the average grain size and standard deviation. Energy-dispersive spectroscopy (EDS) analysis was performed in the SEM for phase identification.

The measurement of grain boundary character distribution (GBCD) in terms of Σ was conducted by using orientation imaging microscopy (OIM™). Electrolytic polishing with a 15% HCl and 85% CH_3OH electrolyte was used to prepare OIM specimens. OIM was conducted on a Phillips XL-30 Environmental SEM equipped with an Argus-20 real-time image processor coupled with Channel 4.2 software to control electron backscatter diffraction (EBSD) acquisition and manipulate, analyze, and display EBSD data. Beam scanning coupled with SEM dynamic focusing was conducted to acquire electron backscatter patterns (EBSPs) of areas of interest to generate relevant image mapping. Results of GBCD, such as fraction of special GBs and high-angle GBs were obtained from the mapping by using Channel 4.2 analyzing software (Ref. 10).

Results and Discussion

Thermal simulation using long-term isothermal solution heat treatment for the multiple-cycle heat treatment produced comparable microstructure, grain size, and hardness levels in the Waspaloy material evaluated, as shown in Table 2. Similar experiments performed with Alloy 718 and IN939™ provided similar results and reinforced the use of isothermal heat treatments to simulate multiple thermal cycles (Ref. 6). Consequently, long-term (40 h) isothermal heat treatments at 1079°C (1975°F) were applied to bulk materials, from which the Gleeble hot-ductility specimens were produced.

Typical Gleeble hot-ductility "signatures" for the Waspaloy material are shown in Fig. 1. These curves demonstrate the change in ductility during both on-heating and on-cooling simulated weld thermal cycles. For the quantitative evaluation of liquation cracking susceptibility, a few critical values are determined. Table 3 lists these values in terms of nil ductility temperature (NDT), nil strength temperature (NST), ductility recovery temperature (DRT), and liquation temperature range (LTR), where LTR is the difference between NST and DRT. Within the LTR, the materials show no ductility during cooling. Therefore, the LTR value can be used to quantify susceptibility to liquation cracking, with larger values indicating higher susceptibility. For comparison, a temperature range of T_p–DRT is also listed, where T_p is the peak temperature for on-cooling test. T_p is determined approximately at the midpoint of NST and NDT for each material.

For both Waspaloy bar and disk materials, the Gleeble hot ductility results indicate the susceptibility to liquation cracking increased after the 1079°C/40-h treatment (Table 3), which represents the case of multiple PWHT in the repair process. The bar material showed slightly deteriorated weldability while the disk showed a drastic degradation in weldability, as indicated by the increase in LTR from 126 to 270°C.

Fractography revealed the fracture

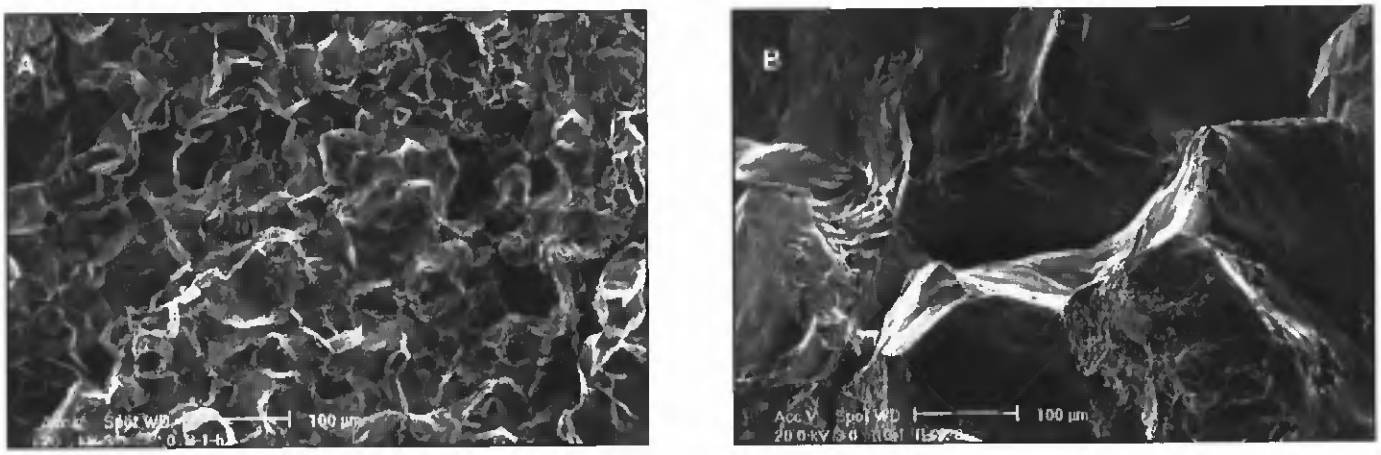

Fig. 3 — Fractography of DRT samples of Waspaloy disk showing IG features. A — As-received; B — 1079°C/40-h treated.

morphology is intergranular (IG) in samples of both the bar and disk tested above DRT and NDT, as shown in Figs. 2 and 3, respectively. This clearly indicated high-temperature GB weakening is the major contributor to failure. Besides, the coarse-grained fracture surface also revealed the effect of the long-term isothermal treatment on the microstructure. Microstructural analysis suggested such GB weakening is caused by two simultaneous liquation phenomena in the simulated HAZ of Waspaloy materials, i.e., carbide constitutional liquation and segregation-induced GB liquation — Fig. 4. From Figs. 4A and B, it can be seen that constitutional liquation and GB penetration is associated with the interaction of Ti-rich MC carbides and the γ-nickel matrix, from which a reaction zone formed, resulting in the formation of eutectic carbides. The typical segregation-induced GB liquation for both bar and disk materials is shown in Figs. 4C and D. The coarse GB constituents are complex boron-rich (around 50 at.-%) eutectics, detected by EDS of the area. Based on the metallurgical analysis, it can be summarized this weldability degradation is primarily related to coarse intergranular fracture due to increased grain size resulting from the long-term isothermal heat treatment.

Grain size is a well-known factor influencing material properties. With regard to the weldability degradation described above, larger grain size represents less grain boundary area and correspondingly fewer triple junctions among grains (Refs. 11, 12). The propagation resistance for liquation cracking with IG features in coarse-grained material (1079°C/40h) was therefore reduced.

Since the Waspaloy disk showed drastic weldability degradation with increasing grain size as a response to 1079°C (1975°F)/40-h thermal effect, the 100-h treatment at 1079°C (1975°F) in the box furnace with air cooling was conducted on the disk material to determine if further weldability degradation occurred. Comparing the LTR values of the disk material in Table 3, it is obvious that, tested with the same T_p level as that of 1079°C/40-h treated Waspaloy disk, 1079°C/100-h treated samples showed a reduced LTR and a corresponding lower (T_p–DRT)

Table 1 — Chemical Composition of Waspaloy Materials

Element	Bar, wt-%	Disk, wt-%	Element	Bar, wt-%	Disk, wt-%
C	0.049	0.033	Al	1.32	1.27
Mn	0.02	0.02	Zr	0.05	0.07
Si	0.08	0.03	V	0.06	
S	<0.003	<0.003	Nb	0.07	
P	<0.01	<0.01	B	0.002	0.005
Fe	1.09	1.52	W	0.13	
Cu	0.02	0.01	Ta	<0.01	
Co	12.95	12.23	Cr	19.09	18.34
Mo	4.09	3.69	Ni	Rem.	Rem.
Ti	2.85	3.12			

Table 2 — Comparison of Grain Size, Hardness, and Microstructural Features for the Thermal Simulation

Waspaloy	Heat Treatment Condition	Grain Size (d_i), µm		Hardness HV1	Microstructural Features
Bar	As-received	14.8 ± 5.8		296.8 ± 1.8	
	1079°/4h-10 cycles	146.8 ± 59		326.4 ± 3.4	Grain growth;
	1079°C/40h	144.5 ± 58		325.6 ± 2.5	MC carbide
	1079°C/40h (BF)	145.2 ± .49		339.2 ± 7.0	stringers
Disk (bimodal grain structure)	As-received (aged)	189 ± 114	46 ± 24	398.4 ± 5.4	
	1079°/4h-10 cycles	532 ± 107	273 ± 88	277.2 ± 26.13	Grain growth;
	1079°C/40h	559 ± 182	255 ± 86	272.9 ± 18.3	equiaxed grain with annealing twins.

Table 3 — Results of Gleeble Hot Ductility Testing of Waspaloy Materials

Waspaloy	Condition	NDT (°C)	NST (°C)	DRT (°C)	Peak Temp (T_p) (°C)	LTR (°C)	T_p–DRT (°C)
Bar	As-received	1246	1302	1093	1280	209	187
	1079°C/40 h	1253	1302	1065	1280	237	215
Disk	As-received	1243	1330	1204	1286	126	82
	1079°C/40 h	1232	1308	1038	1270	270	232
	1079°C/100 h	1232	1303	1218	1270	85	52

Note: LTR = NST-DRT.

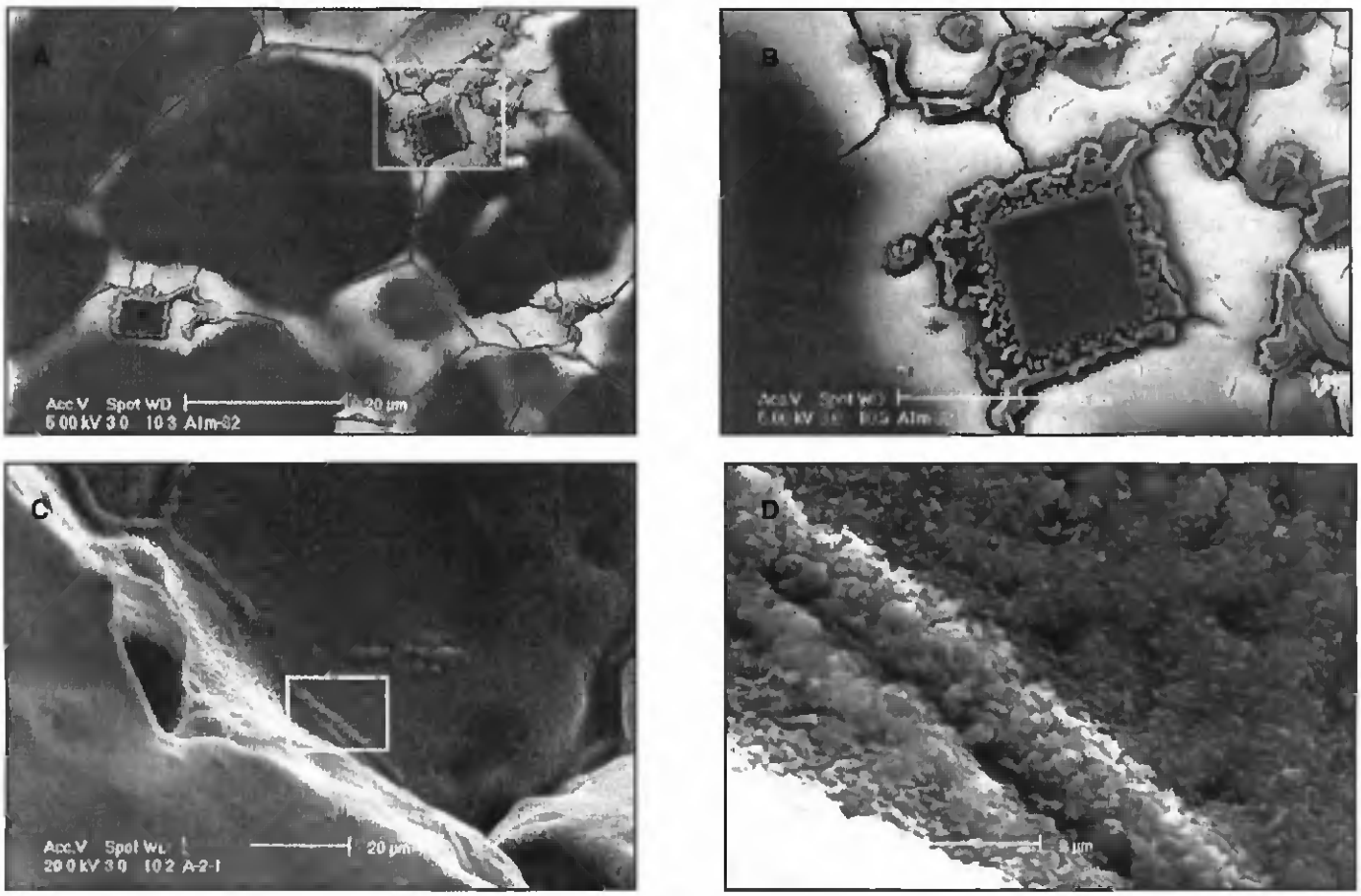

Fig. 4 — Evidence of liquation phenomena in NST samples. A — Carbide constitutional liquation; B — liquation reaction zone around a MC carbide in A; C — GB liquation; D — detail of C showing boron-rich GB constituents.

Table 4 — Grain Size and Distribution of Waspaloy Disk Material.

Waspaloy Disk	Large Grain Size µm	Large Grain Area (%)	Small Grain Size (d_i), µm	Small Grain Area (%)	Area Ratio of Large to Small Grain
As-received	189.1 ± 114	43.8	46.4± 24	56.2	0.78
10798C/40h	559 ± 182	64.7	255 ± 86	35.3	1.83
10798C/100h	586 ± 171	71.5	250 ± 87	28.5	2.51

Table 5 — Grain Boundary Character Distribution (GBCD) of the Waspaloy Disk Material

GBCD (%)	As-Received	1079°C/40h	1079°C/100h
S3	39.7	51.7	65.8
S3, <111>/60°-Twin	38.0	49.6	64.9
S9 and S27	2.3	1.43	0.75
Total $\Sigma \leq 29$	45.6	56.2	69.4
Random	54.4	43.8	30.6

value. This indicates an improvement in weldability after isothermal treatment of 1079°C/100-h relative to 40-h-treated material. Note that T_p affects the ductility of on-cooling samples, including the DRT value, which was observed in the experiments. Therefore, it can be reasonably expected the as-received disk should have an even smaller LTR at least equivalent to that of 1079°C/100-h-treated Waspaloy disk if the same T_p was applied.

The grain size and distribution of 1079°C/100-h-treated Waspaloy disk were acquired as shown in Table 4, along with those of other two conditions of the disk materials. It is noted there is a slight grain size increase for the 1079°C/100-h-treated disk. Besides, there is also a notable increase of fraction of large grains relative to the small ones for the 100-h-treated samples compared with the 40-h-treated ones and the as-received. It is, therefore, clear the improved resistance to liquation cracking of the 1079°C/100-h-treated Waspaloy disk cannot be explained by a grain-size effect. Fractographic and microstructural features were examined to explore potential causes for such an improved resistance. It was observed annealing twins were abundant in the 1079°C/100-h-treated Waspaloy disk samples. Figure 5 shows representative twin-related fracture morphology of samples tested above the DRT, as evidenced by wavy features on the intergranular fracture surface. Inspection of the microstructure revealed some grain boundary segments are resistant to IG fracture.

This is illustrated clearly in 1079°C/100-h-treated Waspaloy disk samples as shown in Fig. 6. It can be seen the crack propagation along GBs ceased at some twin-related segments (Figs. 6, A and B). Wavy dimple-shaped fracture pattern was also seen on the segment interfaces (Fig. 6A), which corresponds to the phenomena observed in Fig. 5. The grain boundary character distribution (GBCD) was therefore evaluated using OIM to

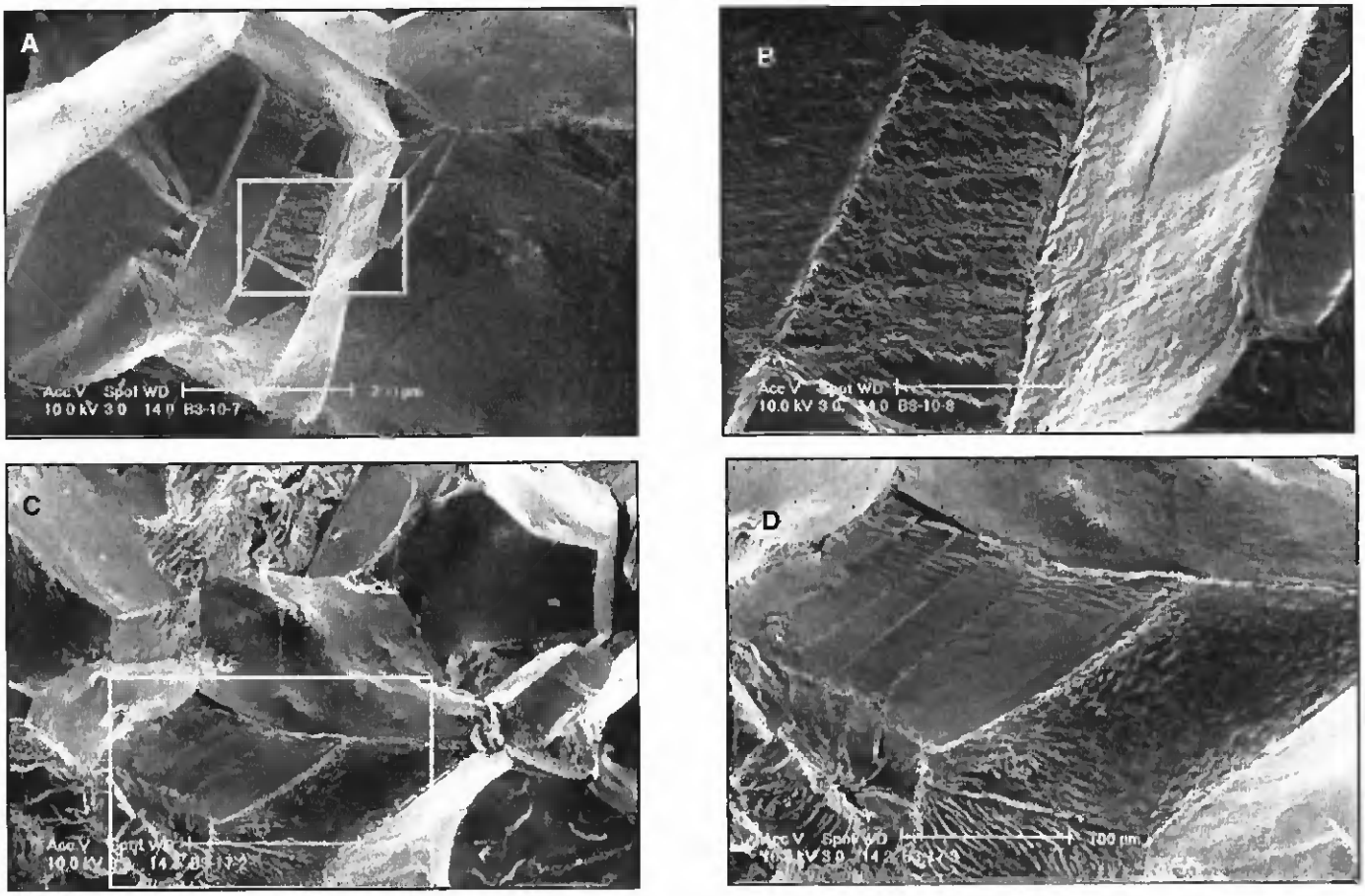

Fig. 5 — Twin-related "wavy" fracture surfaces of 1079°C/100-h-treated Waspaloy disk hot-ductility samples. A — NDT; B — detail of A; C — on-cooling at 1024°C; D — detail of C.

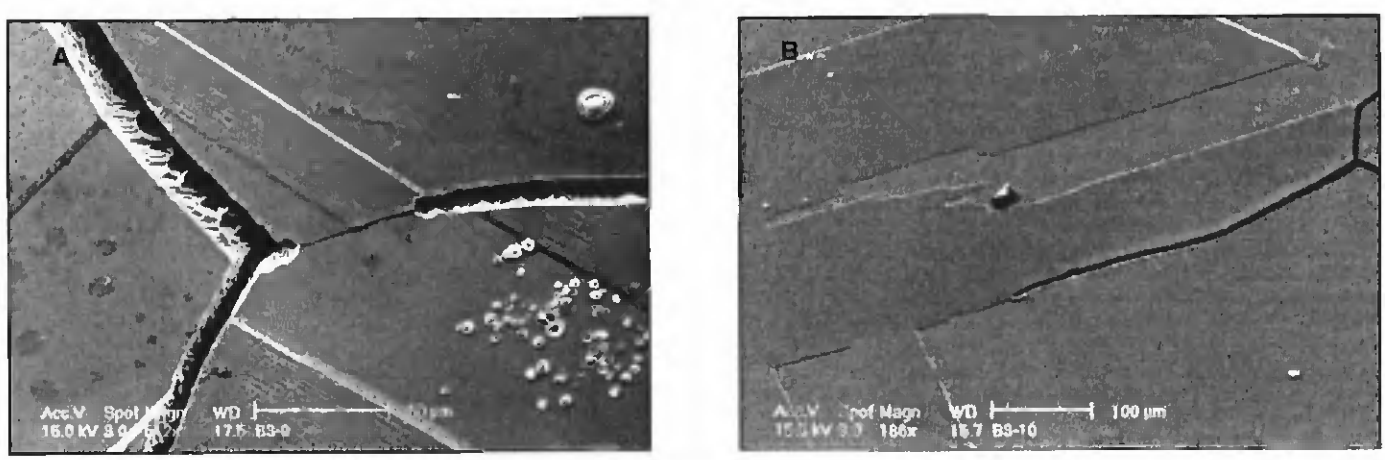

Fig. 6 — Grain boundary (GB) segments resistant to IG fracture in 1079°C/100-h-treated Waspaloy disk. A — Sample tested between NDT and NST; B — NDT sample showing twin-related GB segments hindering the fracture propagation.

quantify the twinning effect.

The acquired volume fraction of GBCD differentiated as Σ3 CSL (Coincidence-Site-Lattice) boundaries, special GBs (Σ<29), and random GBs are shown in Table 5. The values are percentages of the particular boundary in the total boundary length. It can be seen that the fraction of Σ3 CSL boundaries represents the majority of the total special grain boundaries. The fraction of special GBs of the Waspaloy disk materials increased with an increase of the isothermal hold duration, where 1079°C/100-h treatment yielded the highest fraction of special GBs. Since HAZ liquation cracking is intergranular due to the GB liquation that occurred at high temperatures, the behavior of special GBs was investigated. These special GBs have been previously reported to be beneficial to IG degradations as well as weldability (Refs. 11–15).

Figure 7 presents a typical SEM micrograph and the matched OIM image showing boundary orientation. It can be seen some GB segments of an individual GB do not show signs of liquation while others do. GB segments 2, 4, 5, 7, and 8 are not liquated. Note segments 2, 4, and 5 are the interseeted parts of two different pairs of

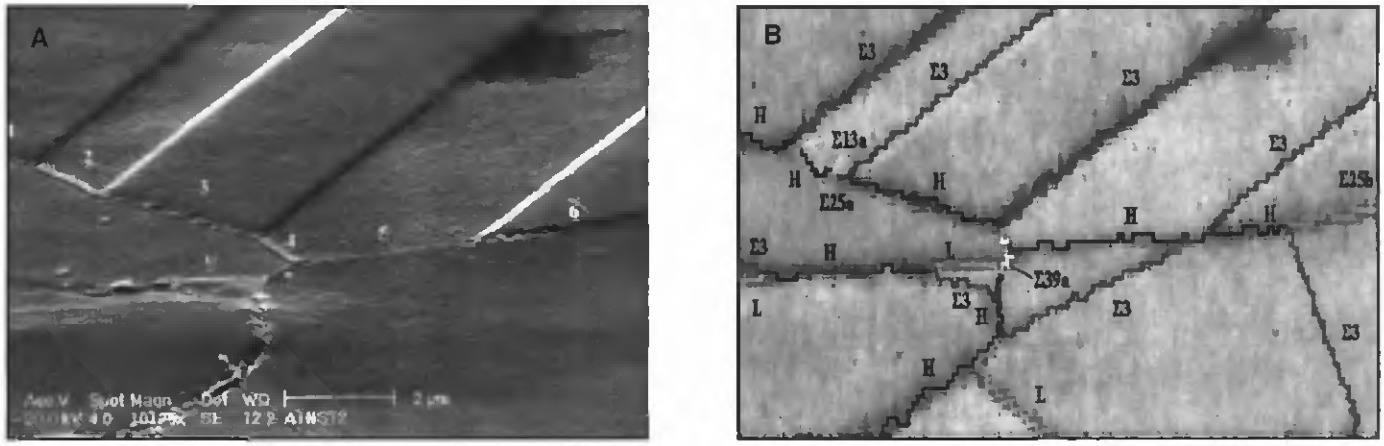

Fig. 7 — Boundary differentiation of Waspaloy bar. A — SEM micrograph; B — OIM image: H– high-angle GB; L– low-angle GB.

twin boundaries with two respective, original high-angle GBs, as shown in Fig. 7B. Segment 2 is composed of sections of special GBs (Σ13a and Σ25a) and high-angle GBs, while segment 4 comprises several sections of Σ CSL boundaries (i.e., Σ13a, Σ25a, and Σ37a). Segment 5 is simply a high-angle GB, however, intersected by a twin. The other two segments, 7 and 8, are not liquated and are identified as Σ39a and a low-angle GB, respectively. It can be summarized, based on the microstructural and OIM analysis, that the increase of resistance to liquation and therefore resistance to IG fracture is closely related to the beneficial effect of special grain boundaries. The Σ CSL GBs, low-angle GBs, and even twin-related, high-angle GBs also showed resistance to liquation.

It is evident, therefore, that a high volume fraction of special GBs, especially Σ3 boundaries, generated in the Waspaloy disk through 1079°C/100-h treatment accounted for the improved weldability. With regard to effects on HAZ liquation cracking, this study has shown both grain size and special GBs have an important influence, but the GBCD can have a dominant effect. Even with relatively large grain size, the cracking susceptibility of the disk material was significantly reduced by increasing the fraction of special GBs. This suggests grain boundary engineering (GBE) techniques can be used to improve the weldability of wrought Waspaloy materials exposed to multiple PWHT cycles following weld repair.

Conclusions

1) The weldability degradation of Waspaloy materials in 1079°C/40-h condition is primarily due to increased grain size from long-term reheats. Finer grain size accounts for the minimal degradation of weldability in the wrought bar, while coarse grains resulted in a drastic deterioration of weldability in the forged disk.

2) Local Ti-rich, MC-type carbide constitutional liquation and segregation-induced grain boundary liquation are responsible for HAZ liquation cracking behavior.

3) The 1079°C/100-h treatment restored the weldability of the Waspaloy disk, even with comparable coarse grain size to that of 1079°C/40-h-treated material. This improvement resulted from the high fraction of special grain boundaries resulting from this heat treatment.

4) Grain size and special grain boundary are the two primary factors influencing HAZ liquation cracking after multiple PWHTs. The presence of abundant special grain boundaries dominated the effect of grain size in the heat-affected zone of the Waspaloy bar stock and the forged disk.

Acknowledgments

Sincere appreciation is expressed to Edison Welding Institute for research funding and Pratt and Whitney for providing some experimental materials.

References

1. Chou, C. P., and Chao, C. H. 1988. Repair weldability studies of Alloy 718 using versatile Varestraint test. *Superalloys 1988*, pp. 785–794. The Metallurgical Society/AIME.

2. Lippold, J. C., Mehl, M., Lu, Q., Lin, W., and Kelly, T. J. 1996. Effect of composition, microstructure, and thermal treatment on the repair weldability of Alloy 718. *77th Annual AWS Convention Abstracts*, pp. 124–125. Miami, Fla.: American Welding Society.

3. Hooijmans, J. W., Lippold, J. C., and Lin, W. 1997. Effect of multiple postweld heat treatment on the weldability of Alloy 718. *Superalloys 718, 625, 706 and Various Derivatives*, pp. 721–730. Minerals, Metals and Materials Society/AIME.

4. Mehl, M. E., and Lippold, J. C. 1997. Effect of δ-phase precipitation on the repair weldability of Alloy 718. *Superalloys 718, 625, 706 and Various Derivatives*, pp. 731–741. Minerals, Metals and Materials Society/AIME.

5. Bowers, R. J., and Lippold, J. C. 1997. Effect of composition and heat treatment cycles on the repair weldability of Alloy 718. *Joining and Repair of Gas Turbine Components*, pp. 41–50. Materials Park, Ohio: ASM International.

6. Qian, M. 2001. An investigation of the repair weldability of Waspaloy and Alloy 718. Ph.D. dissertation. The Ohio State University, Columbus, Ohio.

7. *Waspaloy, Alloy Digest*. 1967. Filing Code: Ni-129.

8. Lin, W., Lippold, J. C., and Baeslack, W. A. III. 1993. An evaluation of heat-affected zone liquation cracking susceptibility, part 1: development of a method for quantification. *Welding Journal* 72(4): 135-s to 153-s.

9. Image Tool 1997. Program developed at the University of Texas Health Science Center at San Antonio, Texas. Available at *http://www.ddsdx.uthscsa.edu*

10. Channel 4.2 software electronic files. 2000. Developed by HKL Technology, Inc.

11. Palumbo, G., King, P. J., Aust, K. T., Erb, U., and Lichtenberger, P. C. 1991. Grain boundary design and control for intergranular stress-corrosion resistance. *Scripta Metallurgica et Materialia* 25: 1775–1780.

12. Cheung, C., Erb, U., and Palumbo, G. 1994. Application of grain boundary engineering concepts to alleviate intergranular cracking in Alloy 600 and 690. *Materials Science and Engineering* A 185: 39–43.

13. Palumbo, G. 1997. Thermomechanical Processing of Metallic Materials. U.S. patent No. 5,702,543.

14. *Manufacturing Process for Enhancing Weldability and High Temperature Performance of Superalloys*. 1998. Integran Technologies.

15. Lehockey, E. M., and Palumbo, G. 1997. On the creep behavior of grain boundary engineered nickel. *Materials Science and Engineering* A 237: 168-172.